Hindawi
International Journal of Aerospace Engineering
Volume 2019, Article ID 2576568, 13 pages
https://doi.org/10.1155/2019/2576568

Research Article

Experiment on the Breakup of Liquid Jets in Different Cross-Airflows

Tian Deng, Wei Chen, Xing-ming Ren, Shuai Jiang, and Chao-hua Yuan

Sino-European Institute of Aviation Engineering, Civil Aviation University of China, Tianjin 300300, China

Correspondence should be addressed to Tian Deng; dengtian.siae@foxmail.com

Received 6 February 2019; Revised 1 May 2019; Accepted 12 May 2019; Published 1 July 2019

Academic Editor: Angel Velazquez

The experiment is conducted with a high-speed camera to investigate the breakup processes of liquid jets in uniform, shear-laden, and swirling cross-airflows. The liquid used in the test is water, the nozzle diameter is 2 mm, and the liquid-to-air momentum flux ratio q ranges from 5 to 3408.5. The results indicate that liquid jets break up to form small droplets in the uniform cross-airflow. There is an exponential relation between the broken position and q. In the shear-laden cross-airflow, the penetration depth of the jet is similar to that of the uniform case, both of which increase with the increase of q. When q and the mean Weber number are the same as the uniform case, the penetration depth of the jet increases by 25% when the velocity ratio of the upper and lower inlets is UR = 5; the jet penetration depth decreases by 47.2% when the ratio of UR = 0.2 and the jet breaks up quickly and the atomization effect will be better. In the swirling cross-airflow, the jet trajectory is similar to the uniform case and also satisfies the exponential property. When the swirl is weak (swirling number $S_N = 0.49$), the jet penetration depth increases compared to the uniform case; when the swirl is strong ($S_N = 0.82$), the cross-swirling airflow restrains the jet penetration depth.

1. Introduction

In recent years, the leading gas turbine companies of the world have begun research on low-NOx emissions under high-thrust conditions. After decades of development, several researches have been achieved in low-emission advanced combustion technology [1]. The lean direct wall injection (LDWI) technology directly injects the fuel jet into the gas or air, and its temperature is not only more uniformly distributed in the main combustion zone but also lower, which has the application prospect of effectively reducing NOx. In the LDWI combustor, the breakup and atomization of the liquid jet in the cross-flow directly affects the combustion efficiency and temperature distribution, but the breakup and atomization models of the jet have not yet reached a unified conclusion. Therefore, more theoretical and experimental research remains needed in the future.

Inamura et al. [2] found that the liquid jet will bend into the cross-flow until the surface breaks into small droplets. Wu et al. [3] observed by experiment that the liquid jet in the cross-flow eventually splits into a liquid belt and further small-sized droplets. A follow-up study by Wu et al. [4] summarized the breakup mechanism, including column breakup, bag breakup, composite breakup, and shear breakup. Tambe et al. [5] and Becker [6] found the parameters that have important correlation with the liquid jet breakup in the cross-flow, the Weber number We and the liquid-to-air momentum flux ratio q, respectively.

Becker and Hassa [7] measured liquid fuel injection into a lean premixed preevaporative combustion combustor with a double annular reverse swirler to study the effects of fuel density and fuel flow on the jet breakup and found that fuel droplets can follow the cross-flow path. Gong et al. [8] studied the experiment of a water jet into a rotating cross-flow and the breakup phenomenon of the jet by changing the number of swirls of the cross-flow, the diameter of the jet nozzle, and the jet velocity. There is no uniform conclusion about liquid jet breakup in the cross-flow from only a few research results, so it cannot be used to guide engineering practice. In this paper, two kinds of nonuniform cross-flow, namely, shear-laden and swirling cross-flow, are constructed to study the breakup process of a liquid jet in nonuniform airflow and compared with the cases of uniform cross-flow to summarize.

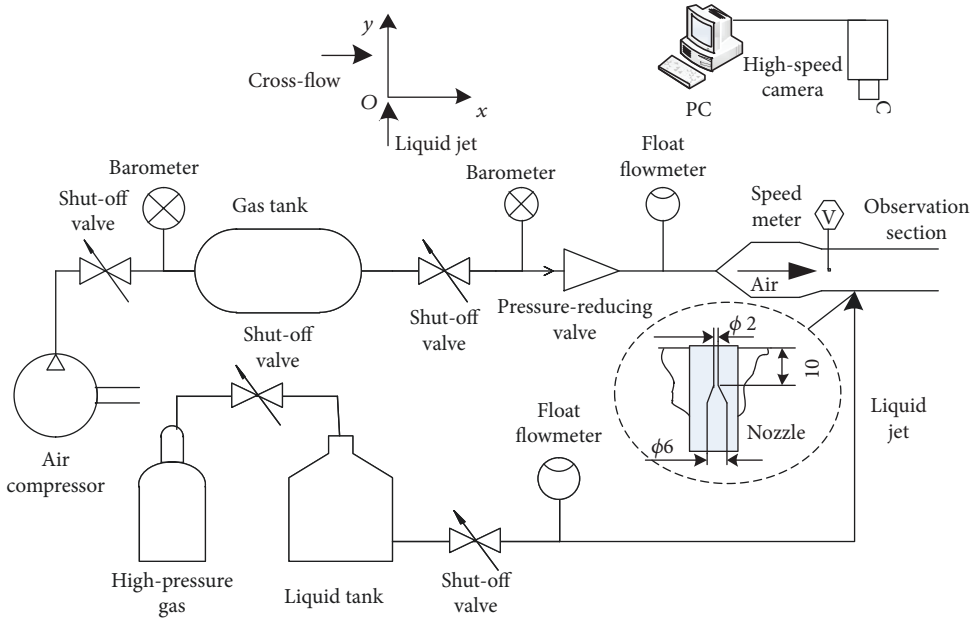

Figure 1: Experimental system scheme.

For computational analysis, since the Eulerian-Lagrangian method is most widely used in academic studies and industrial applications, the main focus is placed on improvement within this framework, especially focusing on primary atomization where modeling is the weakest [9]. Govindaraj et al. [10] investigate the effect of increase in the Weber number at a constant momentum flux ratio on the primary breakup process and the deformation of a kerosene jet in the cross-stream airflow. Unsteady computational analysis with the VOF approach is carried out to simulate the two-phase flow at three different cross-flow Weber number conditions (150, 350, and 400) at a constant momentum flux ratio of 17. With increase in the Weber number, decrease in penetration of the liquid jet along the transverse direction and more bending of the liquid jet along the flow direction are observed. From the velocity profile along the transverse direction of three different conditions, stronger shearing of the liquid film is observed in higher Weber number conditions. Yoo et al. [11] use a three-dimensional large eddy simulation (LES) to investigate the breakup and atomization of a liquid jet into a cross-turbulent flow for several variants of a liquid-gas momentum flux ratio by varying the liquid injection velocity and cross-flow temperature. The spray-field dynamics are treated using a combined Eulerian-Lagrangian approach in which the gas phase is discretized using a density-based, finite-volume approach. A Kelvin-Helmholtz and Rayleigh-Taylor (KH-RT) hybrid wave breakup model is implemented to simulate the liquid column and droplet breakup process.

2. Experimental System

In order to compare the breakup process of the liquid jet in the nonuniform cross-flow, the shear-laden and the swirling cross-flow based on the uniform airflow were designed. The shear-laden cross-flow describes two-dimensional nonuniformity, which is the simplification of three-dimensional nonuniform airflow with a constant axial velocity; the radial velocity is zero; and the tangential velocity is proportional to the radius. A swirler is used to produce a three-dimensional nonuniform cross-flow. The high-speed camera is used to capture the high-frequency picture of the jet, and then the commonality, difference, and influencing factors are processed.

2.1. Experimental System. The experimental system is settled like Figure 1. The maximum air pressure of the storage tank is 0.80 MPa, and the liquid circuit is extruded by high-pressure air. The diameter of the nozzle for uniform flow was $d_1 = 1$ mm and for the others is $d_2 = 2$ mm. The cross-section of the observation section is 84 mm × 84 mm. A hot-wire anemometer is used as the speed meter and an IDT NX3-S4 high-speed camera is used to take photos. In the experiment, the nozzle exit is taken as the coordinate origin, the airflow direction is the x-axis direction (lateral direction), and the liquid jet direction is the y-axis direction (axial direction). The length unit is dimensionless with the nozzle diameter, which means the diameter of the jet is 1 at the exit of the nozzle. The experimental conditions and data collection information are shown in Table 1.

2.2. Experimental Program. Shear-laden airflow is produced by placing a horizontal dividing plate at the center of the entrance of the experiment section, so that two parallel independent cross-flows with different air speeds are introduced into the above and the below partition of the chamber. A numerical simulation method has been used to get more details about the shear-laden airflow field. The CFD software is fluent and the solver is a pressured-based type. The $k - \epsilon$ viscous model has a high accuracy so it is used in this paper. As is shown in Figure 2, when these two cross-flows meet each other, a shear layer is generated at the interface of the

Table 1: Experimental conditions and data information.

Term	Value
Temperature, T (K)	293~298
Liquid density, ρ_L (kg/m^3)	995
Air density, ρ_g (kg/m^3)	1.17
Nozzle diameter, d (mm)	2
Liquid jet velocity, V (m/s)	2-20
Cross-flow velocity, U (m/s)	10-75
Liquid viscosity, μ_L $\left(10^{-6}(\mathrm{Pa}\cdot\mathrm{s})\right)$	866
Liquid surface tension coefficient, σ_L $\left(10^{-3}(\mathrm{N/m})\right)$	70.9
Liquid jet Reynolds number, $\mathrm{Re}_L = (\rho_L V d)/\mu_L$	4500-34500
Cross-flow Weber number, $\mathrm{We}_g = \left(\rho_g U_{g,avg}^2 d\right)/\sigma_L$	10-67
Liquid-to-air momentum flux ratio, $q = \left(\rho_L U_{L,avg}^2\right)/\left(\rho_g U_{g,avg}^2\right)$	5-3408.5
Liquid jet Ohnesorge number, $\mathrm{Oh} = \mu_L/(\rho_L d\sigma_L)^{0.5}$	0.0023
High speed camera exposure time (μs)	16
High speed camera frequency, f	2000

intersection due to the difference in air speed. As the air moves downstream, the thickness of the shear layer increases, creating a quasilinear velocity gradient along the y-axis within the observation section. In addition, since the speed of the upper and the lower cross-flow can be independently controlled, it is possible to generate a situation in which the cross-flow velocity increases (positive gradient) or decreases (negative gradient) with height. The experimental observation section is shown in Figure 3. It is noted that the upper cross-flow velocity is U_a, the lower airflow velocity is U_b, and the upper and lower airflow velocity ratio is $\mathrm{UR} = U_a/U_b$.

The experimental observation section of the swirling cross-flow is mainly composed of two parts, the channel section and the swirler [12]. The observation section is the same as the uniform cross-flow and the shear-laden cross-flow, except that the swirler is installed at the end of the rectifying section. The figuration is shown in Figure 4(a). The swirler can generate a swirling flow whose strength can be characterized by the swirling number S_N, which is defined as follows:

$$S_N = \frac{2}{3}\left(\frac{1-(D_{hub}/D_{sw})^3}{1-(D_{hub}/D_{sw})^2}\right)\tan\theta, \quad (1)$$

where D_{hub} and D_{sw} are, respectively, the swiler hub diameter and the swirler outer diameter and θ is the blade exit direction angle. They are shown in Figure 3. Generally, $S_N > 0.6$ is a strong swirl and $S_N < 0.6$ is a weak swirl. In this test, the swirling cross-flow with $S_N = 0.49$ and $S_N = 0.82$ is realized by changing θ. The experimental program is shown in Table 2. We get the airflow characterization bellowing the swirler of $\theta = 45°$ in Figure 5.

3. Experimental Results and Analysis

3.1. Uniform Cross-Flow

3.1.1. Liquid Column Development and Surface Wave Phenomenon. Since the breakup of the jet liquid column in the cross-flow involves jet characteristics and airflow characteristics [13], the Weber number We and the momentum flux ratio q have an important influence on the development of the jet surface wave and the development of the liquid column. As can be seen in Figure 4, the jet liquid column is broken for the first time at the jet breaking point, and there are droplets generated by the break in the downstream region. The breakup point of the jet is divided into a lateral position and an axial position, as shown in Figure 6.

The liquid column is affected by surface waves, which causes the liquid to develop in an unstable direction. In Figure 7, images of the bag breakup and shear breakup are shown, and Figure 8 is a four-shot continuous jet surface diagram, where jet velocity $V = 5$ m/s, airflow velocity $U = 25$ m/s, airflow average Weber number $\mathrm{We}_{g,avg} = 10.3$, momentum flux ratio $q = 34$. The order of picture collection is (a), (b), (c), and (d).

It can be seen from Figure 8 that the surface of the jet is relatively smooth after being ejected from the nozzle and there is no surface wave. In the downstream, the surface of the liquid column begins to shake and a small amplitude wave can be observed. This wave is extremely unstable and will continue to amplify under the action of cross-flow. Its shape begins to evolve from surface waves to a coherence of body waves and surface waves, and the entire jet liquid column exhibits a spiral flow state. After interaction by the surface wave and the body wave, and under the action of surface tension, the liquid converges toward the peak position, where the jet liquid column breaks and droplets are generated.

To further investigate the generation of surface waves and droplets, Figure 9 magnifies the local portion of the jet column. It can be seen that the size of the large droplets that peeled off of the liquid jet in the cross-flow is about 3.5 times the nozzle diameter, which also proves that the surface wave of the jet liquid column in the cross-flow is more intense. It can concentrate more liquid to the peaks, resulting in larger droplets. When the liquid column is broken to produce large droplets, some small droplets are also generated. The mechanism of these small droplets is similar to that of the jet liquid column in static air to produce droplets, but the difference is that the "satellite droplets" generated by the liquid column will continue to develop downstream under the action of the cross-flow, rather than the satellite droplets in the static air.

At the same time, in Figure 9, the body wave and surface wave exist in the run of the liquid column. Under the action of the cross-flow, the windward and leeward force of the liquid is inconsistent, resulting in the surface wave no longer being a symmetrical wave but being directly in the form of an asymmetric wave, and there are multiorder asymmetric surface waves. At the same time, the body wave is formed in the jet liquid, and it causes the liquid column to flow

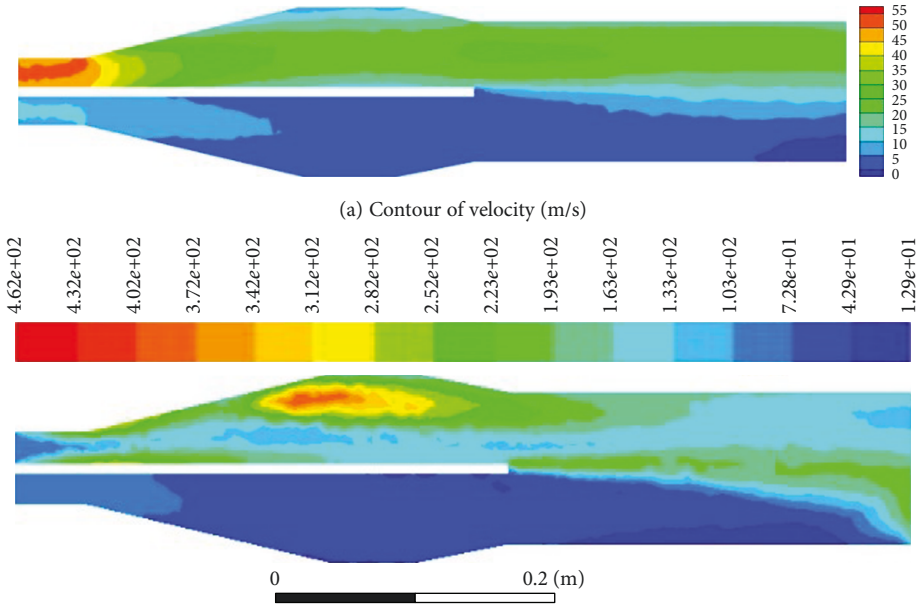

(a) Contour of velocity (m/s)

(b) Contour of turbulence intensity (%)

Figure 2: Typical numerical simulation result.

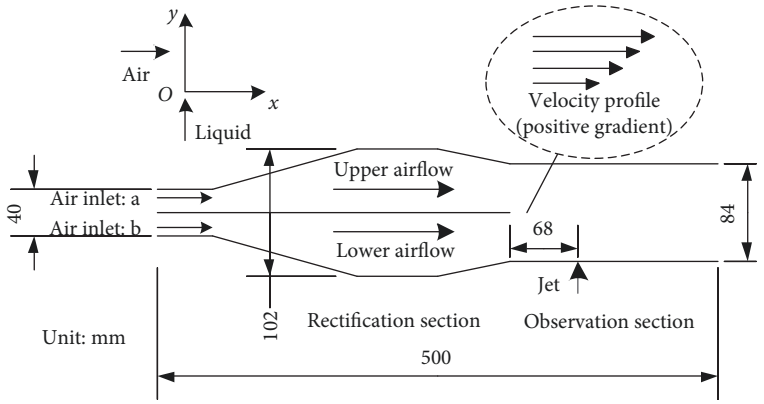

Figure 3: Design of the observation section of the shear-laden cross-flow.

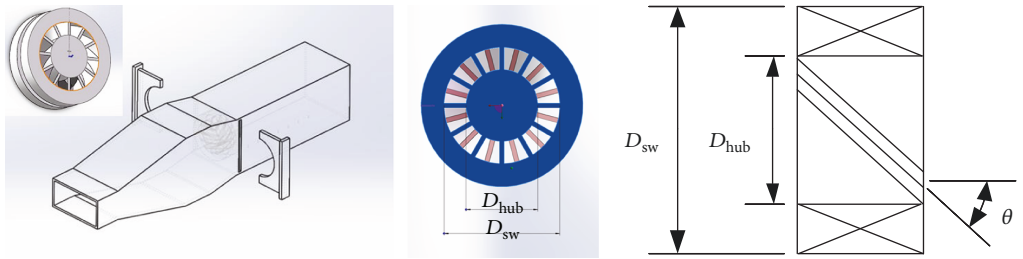

(a) The observation section and swirler

(b) The design parameters of the swirler

Figure 4: Observation section and swirler used in the swirling cross-flow.

downstream in a swirling manner, and the instability of the liquid column is greatly increased.

3.1.2. Correlation of Jet Breakup Position and Jet Trajectory. The analysis of the flow trajectory and the jet breakup position is also a key step for the construction of the jet breakup model in the cross-flow and is a measurement tool for characterizing the breakup of the jet liquid column. The breakup position of the jet is divided into a lateral position and an axial position, as shown in Figure 3.

Table 2: Experimental program.

Experiment no.	Cross-flow	Design parameters	Conditions
1	Uniform cross-flow		
2	Share-laden cross-flow	Upper and lower layer air speed ratio UR	UR < 1 UR > 1
3	Swirling cross-flow	Swirling number S_N	$S_N = 0.49$ ($\theta = 30°$)
4	Swirling cross-flow	Swirling number S_N	$S_N = 0.82$ ($\theta = 45°$)

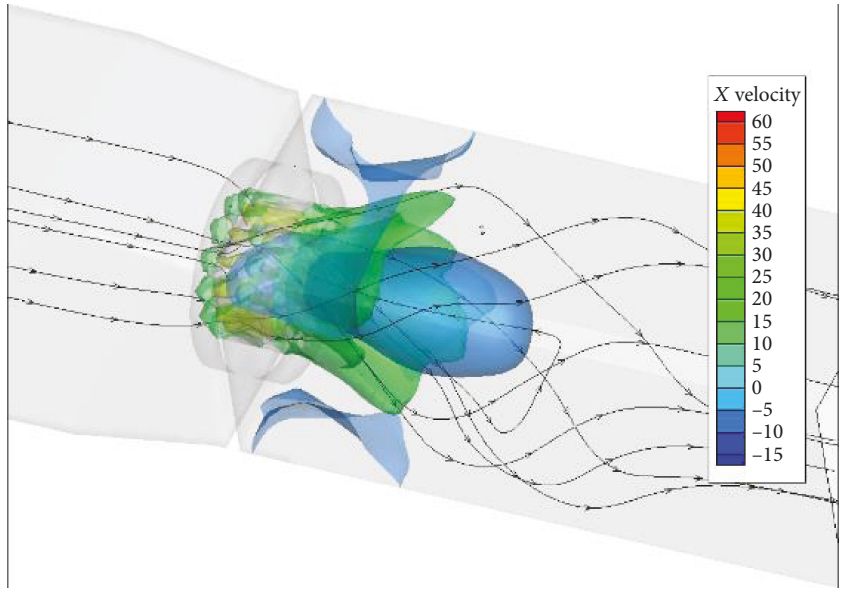

Figure 5: Speed line of $U_g = 10$ m/s, $U_L = 15$ m/s, and $q = 1917.3$.

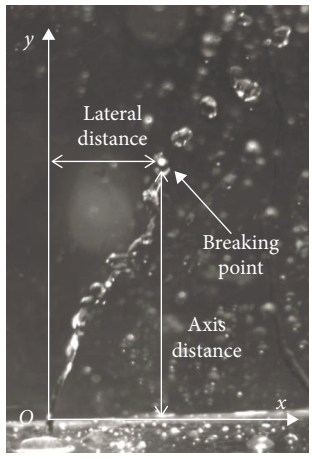

Figure 6: The definition of jet-related parameters.

The breakup position of the jet column mainly depends on the relationship between the air momentum and the liquid jet momentum. Therefore, it is better to study the trajectory and the position of the jet with the liquid-to-air momentum flux ratio q. The results in this section are based on the experimental conditions in Table 3.

The breakup position results are shown in Figure 10.

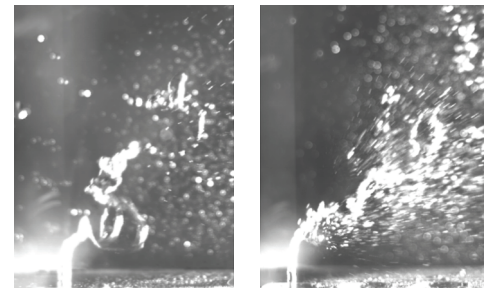

(a) (b)

Figure 7: Phenomena of bag and shear breakup.

The numerical fitting is calculated separately as follows.

(1) Breakup Distance Fitting in the x-Axis Direction. The fitting correlation of the breakup position in the x-axis direction is as shown:

$$\frac{x}{d} = 68.9q^{-0.51}. \quad (2)$$

The experimental and the fitting results are shown in Figure 11.

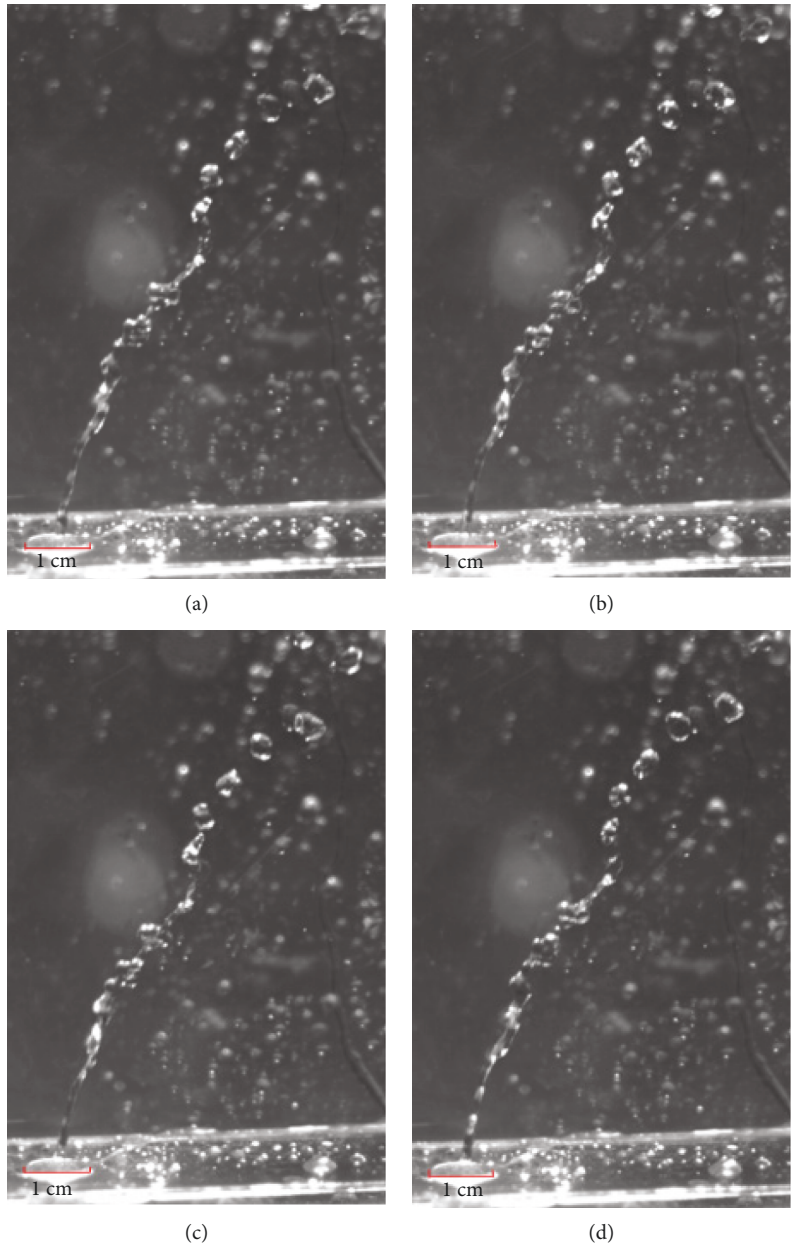

Figure 8: The breakup of the jet liquid column in the cross-flow with $V = 5$ m/s and $q = 34$.

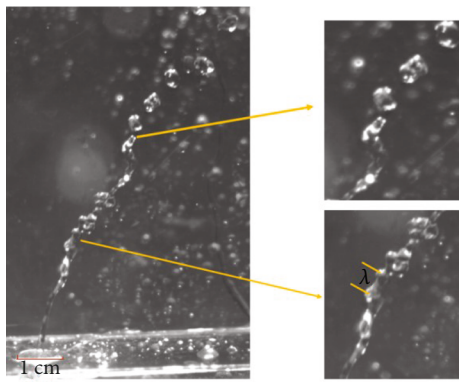

Figure 9: Enlarged view of the surface wave and column fracture.

It can be seen that as the q increases, the lateral breakup distance of the jet decreases. This is due to the increase of aerodynamic force, and the jet surface generates more small amplitude surface waves, which will make the jet column more unstable, and the breaking distance in the lateral direction is reduced.

(2) Breakup Distance Fitting in the y-Axis Direction. The fitting correlation of the breakup position in the y-axis direction is as shown:

$$\frac{y}{d} = 9.96q^{0.27}. \quad (3)$$

The experimental and fitting results are shown in Figure 12.

Table 3: Experimental conditions.

Experiment number	Liquid jet velocity, V (m/s)	Cross-flow velocity, U (m/s)	Liquid-to-air momentum flux ratio, q
1	4	20	34.052
2	4	22	28.14215
3	4	25	21.79328
4	8	25	87.17312
5	8	30	60.53689
6	8	35	44.47608
7	11	30	114.4526
8	11	34	89.10666
9	11	38	71.3347

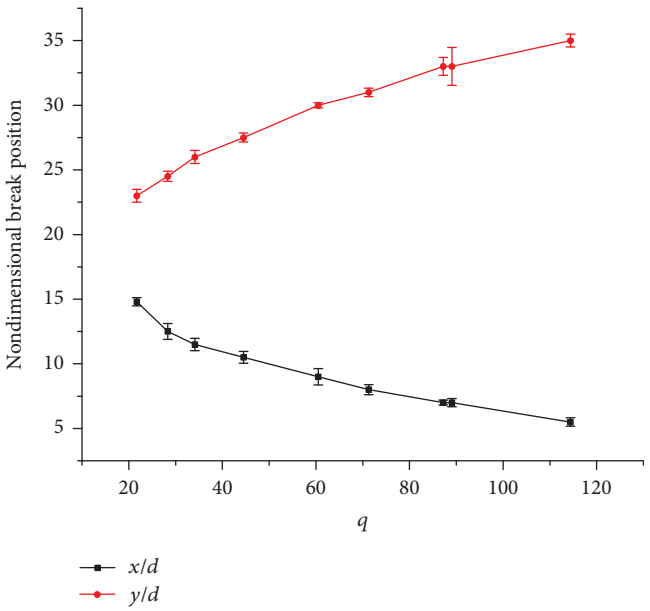

Figure 10: The dimensionless breakup position with q.

The results here are opposite to the decrease in the lateral distance, because the momentum of the jet is sufficient to resist the cross-flow as q increases, so its penetration distance in the y-axis will increase.

(3) Jet Flow Trajectory. On the basis of the lateral and the axial breakup distance, the correlation between the jet flow trajectory and q can be approximated as flow.

It assumes in this part that the velocity of the liquid jet in the y-axis direction is uniform and that there is an aerodynamic force in the lateral direction. Based on this assumption, the trajectory of the jet should appear in the form of a quadratic function; i.e., the square of y/d is quasilinear with x/d. Combining equations (2) and (3), the trajectory of the jet can be obtained as shown:

$$\frac{y}{d} = 1.21q^{0.531}\left(\frac{x}{d}\right)^{0.5}. \quad (4)$$

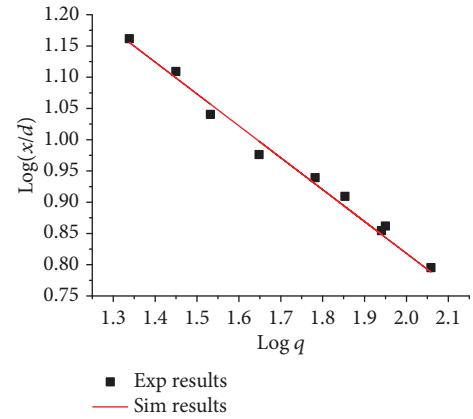

Figure 11: Comparison of the experimental results (Exp results) and the mathematical fitting results (Sim results) in the x-direction breaking point.

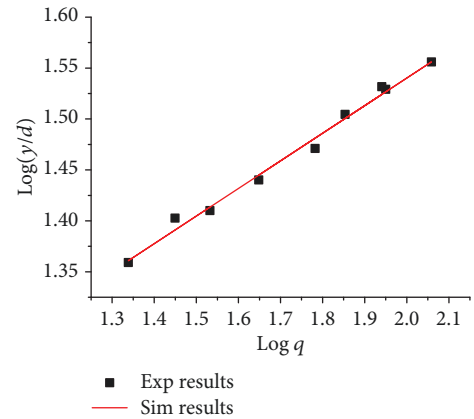

Figure 12: Comparison of the experimental results (Exp results) and the mathematical fitting results (Sim results) in the y-direction breaking point.

3.2. Shear-Laden Cross-Flow. The experiment was operated under the condition that the momentum flux ratio q = 10.53 and the gas average Weber number $We_{g,avg}$ = 66.83 (the average velocity of the cross-flow $U_{g,avg} = \dot{m}/S\bullet\rho_g = (U_a + U_b)/2 = 45$ m/s), where the upper and lower layer speed ratio UR is equal to 0.2, 0.5, 2, and 5. Figure 13 shows the breakup of the liquid jet under these conditions. The thick red line represents the location of the division plate. It can be seen that, in the case where q and $We_{g,avg}$ are kept the same, as the UR value increases, the jet penetration depth increases. This phenomenon occurs because the local cross-flow resistance placed on the liquid jet varies with the height from the nozzle exit.

Figure 14 shows the correlation between the penetration depth of the liquid jet and the UR in the case where q and $We_{g,avg}$ are kept the same. For UR < 1, the liquid jet immediately encounters a very high velocity cross-flow after leaving the nozzle. The liquid-to-air momentum flux ratio q has a lower value, which caused its trajectory to

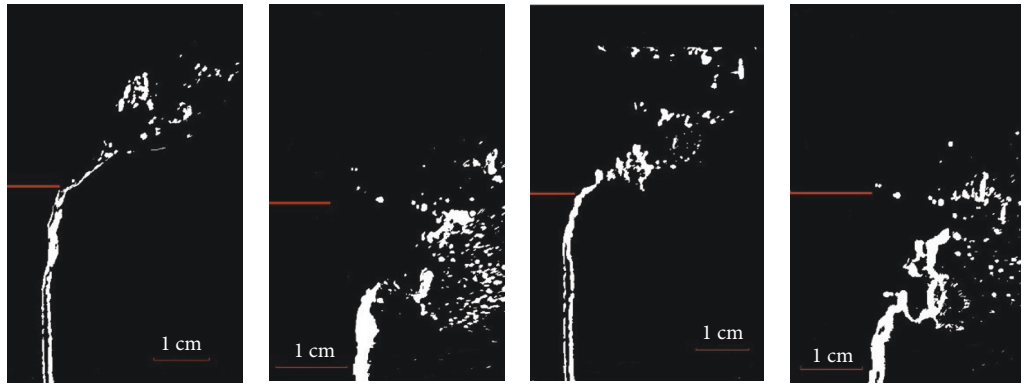

Figure 13: Image of liquid jet breakup: (a) UR = 5; (b) UR = 0.2; (c) UR = 2; (d) UR = 0.5.

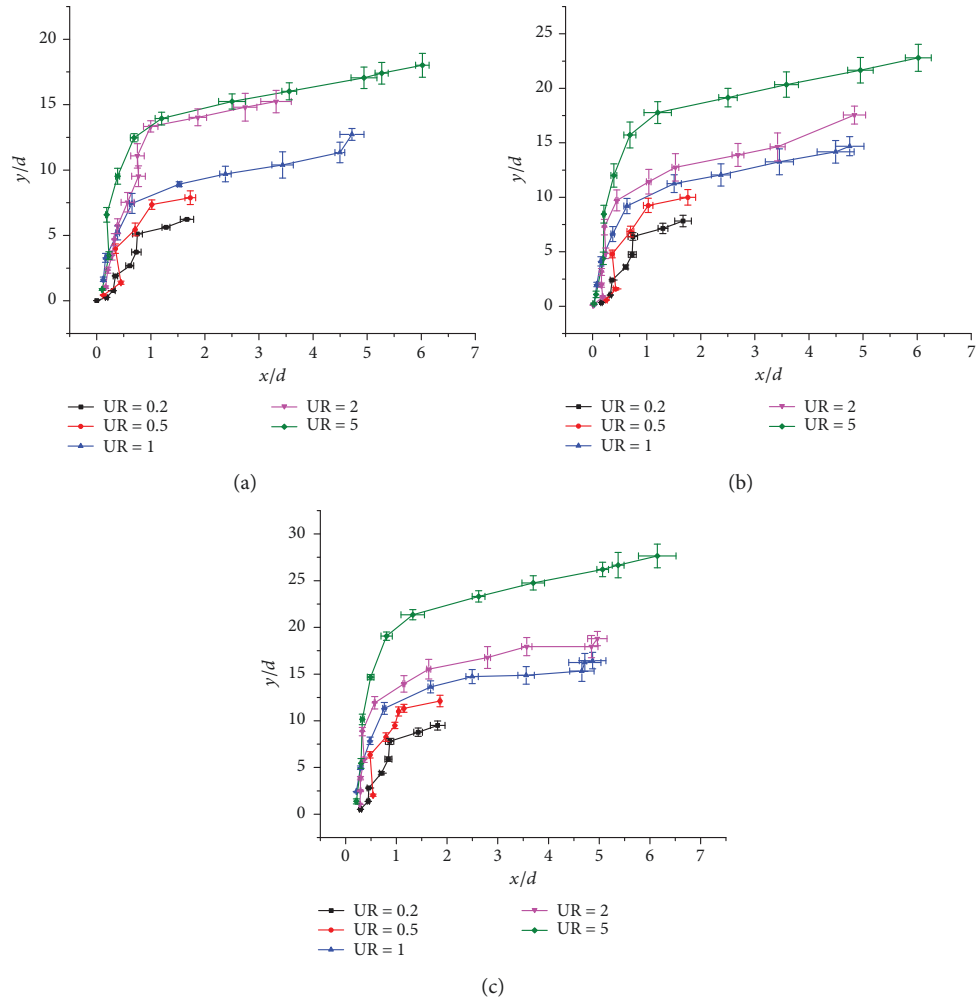

Figure 14: Effect of UR on the penetration depth of liquid jets: (a) $We_{g,avg} = 66.83$, $q = 10.53$; (b) $We_{g,avg} = 66.83$, $q = 23.69$; (c) $We_{g,avg} = 66.83$, $q = 34.12$.

change rapidly, and the overall penetration depth of the liquid jet is also low. However, if the local q is large enough, it is possible for the liquid jet to penetrate the adjacent high-velocity layer of the cross-flow into the lower velocity layer; the resistance is reduced and the penetration depth of the liquid jet is significantly increased. For UR > 1, the cross-flow velocity near the liquid jet nozzle is low, so the local q is large and the penetration depth can be increased. Therefore, even if the average q is lower than 10, the jet can reach a higher layer cross-flow.

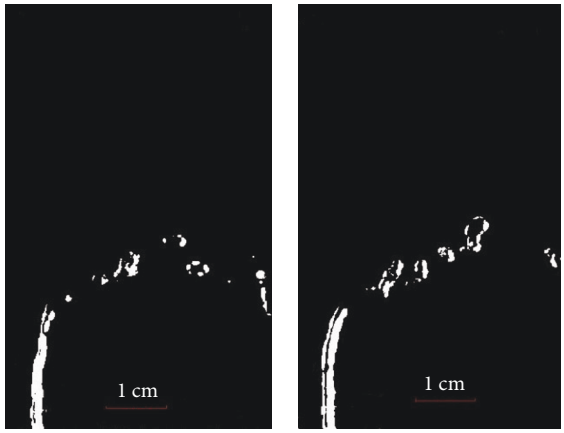

Figure 15: Liquid jet breakup with different $We_{g,avg}$: (a) $We_{g,avg}$ = 29.25; (b) $We_{g,avg}$ = 66.83.

Figure 15 shows the jet trajectory images of the two conditions with UR = 1 and q = 10.53, and the penetration depth is almost the same. It is impossible to correlate the jet penetration depth and the average flow Weber number $We_{g,avg}$.

3.3. Swirling Cross-Flow

3.3.1. Weak Swirling Cross-Flow. The liquid breakup position and the jet trajectory are studied to analyze the movement of the liquid jet in the swirling cross-flow. In this experiment, an axial swirler with a swirling number S_N = 0.49 is installed at the front of the experimental observation section to realize a weak swirling cross-flow. The q of each case is different but with the order of magnitude 10^2. The experimental data is shown in Figure 16; it can be seen that the breakup point of the liquid jet in the swirling flow is closer to the nozzle in the x-axis direction while the distance in the y-axis direction is further away from the nozzle as q is increased.

Fitting the position coordinates of the breakup position with q can obtain two formulas for the x-axis and the y-axis direction, respectively:

$$\frac{x}{d} = 54.35q^{-0.487}, \tag{5}$$

$$\frac{y}{d} = 8.62q^{0.256}. \tag{6}$$

Since both equations (5) and (6) are exponential, a linear relationship function by the logarithmical method can be obtained, as shown in Figure 17.

Based on the position information of the breakup point obtained above, the coordinate equation of the breakup position is derived:

$$\frac{y}{d} = aq^{b}\left(\frac{x}{d}\right)^{c}. \tag{7}$$

The values of the coefficients in equation (7) are a = 1.184, b = 0.498, and c = 0.497, and the correlation is 97%.

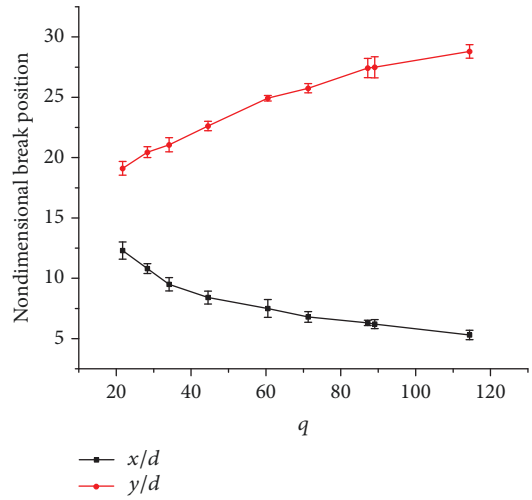

Figure 16: Nondimensional breakup position with q in the swirling cross-flow.

3.3.2. Strong Swirling Cross-Flow. The swirler used in this section is S_N = 0.82, resulting in a strong swirling cross-flow. The liquid-to-air momentum flux ratio q is in the order of 10^3. The data measured is as shown in Figure 18. It can be found that in the case of the strong swirl, the axial distance (y-axis) of the jet trajectory increases while the lateral distance (x-axis) decreases as q increases, and the penetration depth is positively correlated with q. In part of the cases, there is a shake movement in the trajectory, the reason of which will be explained below.

According to the empirical formula of the jet trajectory in the uniform cross-flow in the document [14]:

$$\frac{y}{d} = 1.18q^{0.45}\left(\frac{x}{d}\right)^{0.45}. \tag{8}$$

The jet trajectory can be calculated under the same momentum flux ratio q in the uniform cross-flow. The comparison with the experimental data in Figure 15 is shown in Figure 19. The scatter plot represents the experimental data in the swirling cross-flow. The line graph represents the calculated predicted data in the uniform cross-flow.

It can be clearly observed that the penetration depth of the liquid jet in the swirling cross-flow is lower than that of the uniform cross-flow under the same conditions. The jet trajectory data in Figure 15 shows that the jet column has obvious to-and-fro movement in partial cases, such as cross-flow average velocity $U_{g,avg} = \dot{m}/S\bullet\rho_g$ = 10 m/s, V = 15 m/s, and q = 1917.3. Its experiment image is shown in Figure 20. The low-speed cross-airflow under strong swirling will bring a large recirculation zone, in which air has a negative velocity (x-axis direction). The penetration depth of the liquid jet is suppressed, and the shape of the liquid column is greatly affected. It shows that the liquid jet trajectory prediction formula in the uniform cross-flow needs to be corrected when used to swirling cross-flow.

3.4. Comparative Analysis of the Uniform and the Nonuniform Cross-Flow.

Keeping q and $We_{g,avg}$ the same,

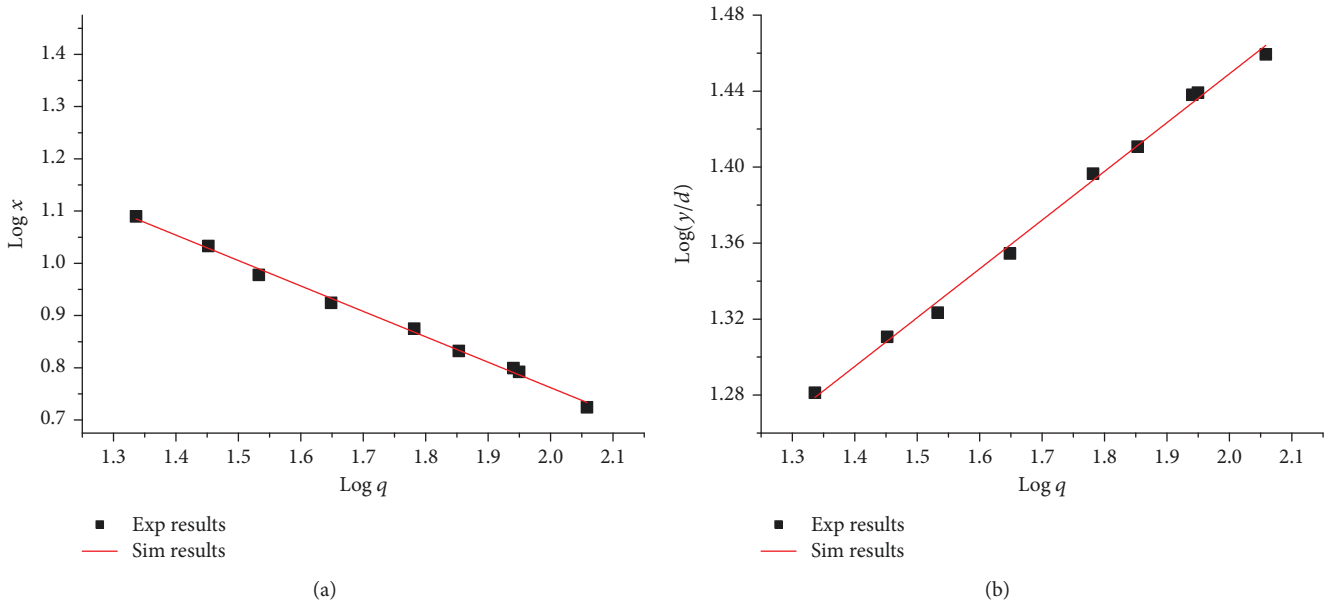

Figure 17: Experiment results (Exp results) and simulation results (Sim results) for the breakup position.

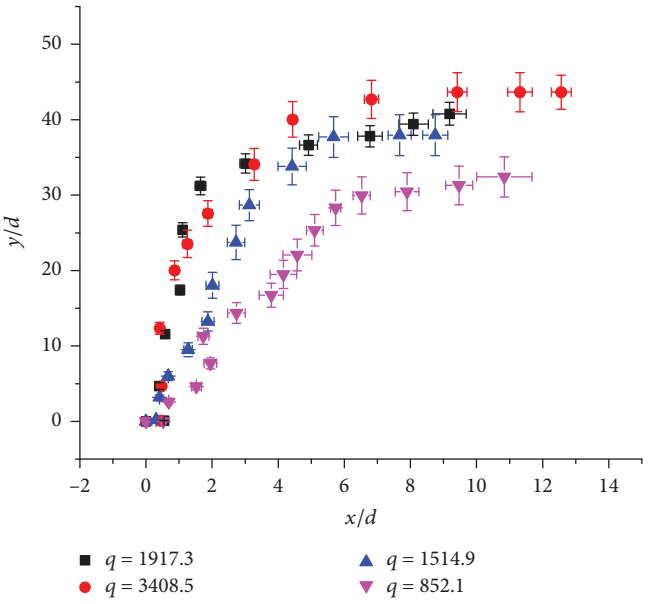

Figure 18: The jet trajectory of different q.

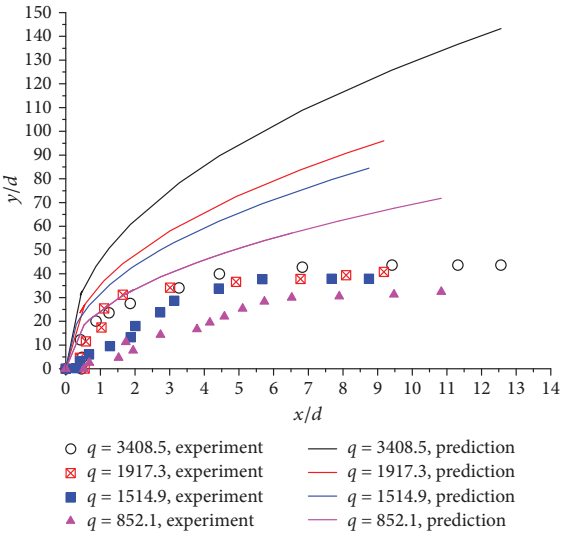

Figure 19: Experimental results and prediction results of the jet trajectory.

the jet penetration depth is about $6d$ when UR = 0.2, $8d$ when UR = 0.5, and $13d$ when the liquid jet is like the uniform cross-flow (UR = 1); the penetration depth of the jet can reach $18d$ when UR = 5, and the slope of the liquid jet trajectory changes very obviously. Therefore, reducing the UR from 1 to 0.2 can reduce the jet penetration depth by 47.2%, and increasing the UR from 1 to 5, the penetration depth of the liquid jet can be increased by more than 25%. It can be concluded that UR has great impact to the liquid jet penetration depth.

For a liquid jet in a uniform cross-flow, the momentum flux ratio q is the main parameter affecting the penetration depth of the jet, and the penetration depth increases as q increases. From Figure 21, we can see when the Weber number $We_{g,avg} = 14.53$ ($U_{g,avg} = 30$ m/s), the airflow velocity ratio UR = 1, and the momentum flux ratio q of 10.53, 23.69, and 34.12, respectively. The penetration depth increases as q increases, which is consistent with the conclusions of the liquid jet in a uniform cross-flow.

The uniform cross-flow and the shear-laden cross-flow have substantially the same jet liquid breakup, and the former can be considered as a special case of the latter. Under the condition of the lower gas Weber number, the UR and momentum flux ratio q have a significant effect on the penetration depth.

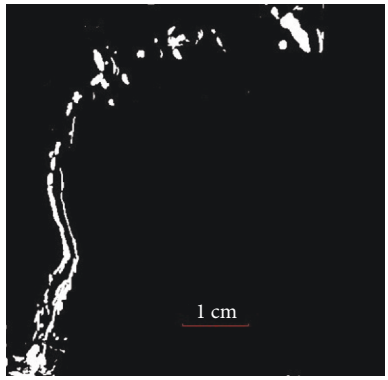

Figure 20: Liquid column fluctuations in uniform cross-flow $U_g = 10$ m/s and $U_L = 15$ m/s.

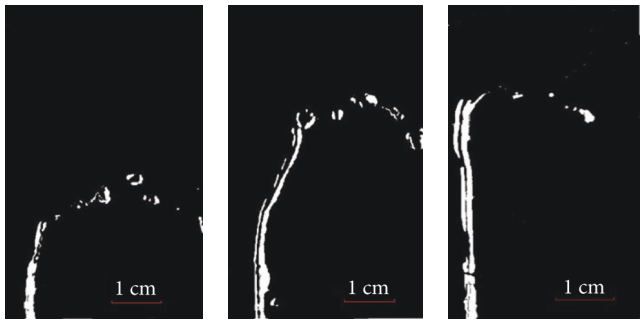

Figure 21: The breakup of the liquid jet of different q: (a) $q = 10.53$; (b) $q = 23.69$; (c) $q = 34.12$.

Comparative results of the jet breakup position between the uniform cross-flow and the swirling cross-flow with $S_N = 0.49$ are shown in Figure 22. It shows that under the same experimental conditions, the breakup position in the swirling is closer to the nozzle outlet because the swirling cross-flow will generate a recirculation zone and there is a negative velocity along the x-axis in the recirculation zone.

The jet breakup mechanism in the swirling cross-flow is generally similar to that in the uniform cross-flow. The jet shape is still in the form of an exponential function. The effect of a weak swirl on the cross-flow is not obvious, and the pressure drop is caused by the airflow after the swirler weakens the aerodynamic force. The liquid column is basically consistent with the trend in the uniform cross-flow, but the penetration depth is slightly improved because the turbulent flow of the swirling flow produces an upward aerodynamic force to the liquid jet. When the order of $q$is low (q~100), there is an exponential relation between the jet breakup position and q. Under the aerodynamic force, the jet is mainly broken by the shear mode. Compared with the uniform case, liquid jet in the strong swirling cross-flow has a lower penetration depth because the strong swirling zone has a larger size, covering the liquid jet recirculation region. The liquid jet is greatly forced by the swirling air, and the kinetic energy of the liquid jet is more converted into air turbulent energy, which inhibits the increase of penetration depth.

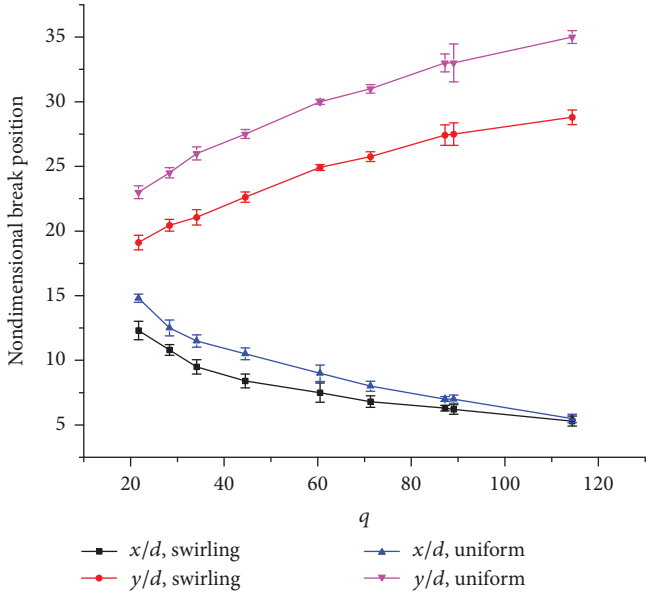

Figure 22: Comparison of the position of the jet breakup in uniform and swirling cross-flows.

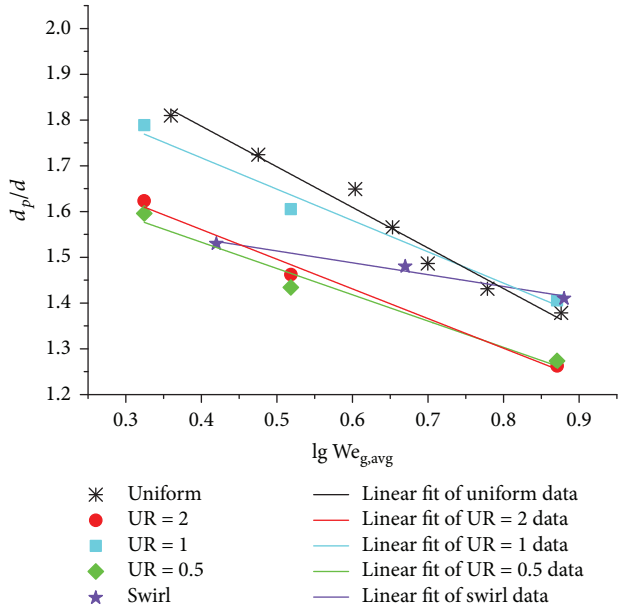

Figure 23: The droplet size distribution in the different cross-flows.

3.5. The Droplet Size Distribution in the Different Cross-Flows. The average diameter of the liquid droplets formed after the jet breaking is an important parameter to the atomization. In this paper, the droplet size distribution after jet breaking in different cross-flows is measured. Since the high-speed camera can only obtain the plane images, the area equivalent method is used to obtain the droplet diameter. That is, the area of the irregular-shaped droplet formed after the breakup is measured, which is equivalent to the circle area, and the corresponding diameter is obtained. Figure 23 shows the relationship between the average dimensionless

diameter d_p/d of the droplets and the average Weber number $We_{g,avg}$ of the cross-flow.

In the uniform lateral airflow, d_p/d decreases with the increase of $We_{g,avg}$ and the points are linearly fitted to obtain a semiempirical relationship:

$$\frac{d_p}{d} = -0.936 \lg We_{g,avg} + 2.18. \quad (9)$$

The linear correlation coefficient of the fitted line is 0.95. We know that when the cross-flow Weber number is less than 10, the breaking of the jet is a bag breakup, and there is no secondary breakup until the Weber number is greater than 14, which is why the jet does not undergo secondary breakup in the experiment and the average diameter of the droplets is large.

In the shear-laden cross-flow, when UR = 1, the nature of the droplets is similar to that of the uniform case. The droplet sizes decrease with the increase of $We_{g,avg}$, while when UR = 2 or UR = 0.5, the droplet sizes formed are generally small. That is to say, the cross-flow velocity gradient will generate vortices in the jet region; the larger the vortex, the greater the impact on the liquid jet breakup. The liquid column breakup process has a mix of bag and shear breakup modes. So the overall droplet diameter will be smaller and the atomization effect is better. The fitted lines of UR = 1, 2, and 0.5 are (10), (11), and (12), respectively, and the linear correlation coefficient is 0.997, 0.97, and 0.96, respectively.

$$\frac{d_p}{d} = -0.558 \lg We_{g,avg} + 1.916. \quad (10)$$

$$\frac{d_p}{d} = -0.665 \lg We_{g,avg} + 1.843. \quad (11)$$

$$\frac{d_p}{d} = -0.594 \lg We_{g,avg} + 1.77. \quad (12)$$

In the swirling cross-flow with the swirl number S_N = 0.49, we can see from Figure 20, when the Weber number is small, that the droplet size distribution is relatively small. The aerodynamic force acting on the jet of swirling cross-flow is more complicated, and there may be a tendency to deflect downward or even upstream for the jet column. It can also be seen that the decrease of particle size is relatively small with the increase of $We_{g,avg}$. Because the three components of the velocity of the swirling cross-flow increase as $We_{g,avg}$ is increasing, and the increment of the forward direction is smaller than the uniform and shear-ladencross-flows. The fitted lines of the swirl case is as (13) and the linear correlation coefficient is 0.96.

$$\frac{d_p}{d} = -0.259 \lg We_{g,avg} + 1.643. \quad (13)$$

4. Conclusions

(1) The liquid jet in the uniform cross-flow will break up to form small droplets. There is an exponential relation between the jet breakup position and liquid-to-air momentum flux ratio

(2) In the shear-laden cross-flow, the upper and the lower inlet velocity ratio UR can describe the velocity gradient distribution of the shear layer and the turbulence of the cross-flow. UR has a great effect on the penetration depth of the liquid jet. When UR > 1, the jet penetration depth is greater than that in the uniform cross-flow when average velocity is the same; when UR < 1, the jet penetration depth is significantly reduced, making the liquid breakup earlier, and the atomization is expected to be better. This is consistent with the conclusions drawn by Tambe [12]. The liquid jet penetration depth in both the shear-laden and the uniform cross-flow increases as the liquid-to-air momentum flux ratio increases

(3) In the swirling cross-flow, the jet trajectory is similar to that in the uniform cross-flow, and both satisfy the exponential characteristics. When the swirl is weak, the penetration depth of the jet is larger than that of the uniform cross-flow; when the swirl is strong, the recirculation zone airflow covers the liquid jet, and the trend of the liquid jet is extremely forced to the direction of the swirling flow, while the kinetic energy of the jet is more converted into air turbulent flow energy, which inhibits the increase of penetration depth

(4) In the shear-laden cross-flow, when UR > 1, the jet penetration depth is large and the liquid jet takes longer to break, and when UR < 1, the penetration depth is lower and the breakup occurs earlier. At the same time, the liquid jet breaks and atomizes better. In addition, the breakup and atomization of the liquid jet in the swirling cross-flow need to consider both the strength of the swirling and the position of the nozzle, which will provide some guidance for the design of the LDWI combustion chamber. For the design of the combustion chamber, it is considered to control the cross-flow and liquid parameters involved in this study to achieve more efficient atomization and reduce pollutant emissions

Data Availability

All the data supporting the results were shown in the paper and can be obtained from the corresponding author.

Conflicts of Interest

The authors declare that there is no conflict of interest regarding the publication of this paper.

Acknowledgments

The work described in this paper is fully supported by a grant from the National Natural Science Foundation of China (No. 51506216) and the Fundamental Research Funds for the Central Universities (No. ZXH2012H001).

References

[1] H. G. Zhong and T. Zhu, "Vaporization and discharge characteristics of lean premixing prevaporizing system," *Journal of Aerospace Power*, vol. 23, no. 7, pp. 1174–1181, 2008.

[2] T. Inamura, N. Nagai, T. Watanabe, and N. Yatsuyanagi, "Disintegration of liquid and slurry jets traversing subsonic airstreams," *Experimental Thermal & Fluid Science*, vol. 7, no. 2, pp. 166–166, 1993.

[3] P. K. Wu, K. A. Kirkendall, R. P. Fuller, and A. S. Nejad, "Breakup processes of liquid jets in subsonic crossflows," *Journal of Propulsion and Power*, vol. 13, no. 1, pp. 64–73, 1997.

[4] P. K. Wu, K. A. Kirkendall, R. P. Fuller, and A. S. Nejad, "Spray structures of liquid jets atomized in subsonic crossflows," *Journal of Propulsion and Power*, vol. 14, no. 2, pp. 173–182, 1998.

[5] S. Tambe, O. Elshamy, and S. M. Jeng, "Liquid jets injected transversely into a shear layer," in *45th AIAA Aerospace Sciences Meeting and Exhibit*, Reno, NV, USA, January 2007.

[6] J. Becker, "Breakup and atomization of a kerosene jet in crossflow at elevated pressure," *Atomization and Sprays*, vol. 12, no. 1-3, pp. 49–68, 2002.

[7] J. Becker and C. Hassa, "Liquid fuel placement and mixing of generic aeroengine premix module at different operating conditions," *Journal of Engineering for Gas Turbines and Power*, vol. 125, no. 4, pp. 901–908, 2003.

[8] X. Gong, K. J. Choi, and N. P. Cernansky, "Lean direct wall injection mode atomization of liquid jets in swirling flow," *Journal of Propulsion and Power*, vol. 22, no. 1, pp. 209–211, 2006.

[9] J. Shinjo, "Recent advances in computational modeling of primary atomization of liquid fuel sprays," *Energies*, vol. 11, no. 11, article 2971, 2018.

[10] M. Govindaraj, M. H. Suryanarayanarao, P. Kotegar et al., "Computational analysis on primary breakup and deformation of kerosene jet in subsonic cross flow using VOF method," in *ASME 2017 Gas Turbine India Conference. American Society of Mechanical Engineers*, p. 11, Bangalore, India, December 2017.

[11] Y. L. Yoo, D. H. Han, J. S. Hong, and H. G. Sung, "A large eddy simulation of the breakup and atomization of a liquid jet into a cross turbulent flow at various spray conditions," *International Journal of Heat and Mass Transfer*, vol. 112, pp. 97–112, 2017.

[12] S. Tambe, *Liquid jets injected into non-uniform crossflow, [Ph. D. thesis]*, University of Cincinnati, 2010.

[13] Y. Lin, L. Li, and C. Zhang, "Progress on the mixing of liquid jet injected into a crossflow," *Acta Aeronautica et Astronautica Sinica*, vol. 35, no. 1, pp. 46–57, 2014.

[14] R. J. Margason, "Fifty years of jet in cross flow research," in *AGARD, Computational and Experimental Assessment of Jets in Cross Flow*, p. 41, 1993.